IN FLIGHT CALIBRATION OF THE ON AXIS AND NEAR OFF AXIS PSF FOR THE MOS1 AND MOS2 CAMERAS.

EPIC-MCT-TN-008 **Simona Ghizzardi**

February 8, 2001

———————————————-

S. Ghizzardi - Milano Calibration Team - Istituto di Fisica Cosmica "G. Occhialini"- CNR - Milano

e-mail: simona@ifctr.mi.cnr.it

Contents

1 Introduction

In this document, I present the results concerning the calibration of the on axis and off axis (up to 2' off-axis) PSF using in orbit data. Data concern both MOS cameras and include observations performed in different operative modes (Full Frame, Double Node, Large Window, Small Window) with different filters.

The document is organized according to the following main topics

- In Sec. 2 I describe the data set used for the calibration;
- In Sec. 3 I describe the procedure for the modelization of the PSF. We fit the PSF with a King profile with two shape parameters: the core radius r_c and the slope α: both of them depend on energy and on off-axis angle;
- In Sec. 4 we provide the Encircled Energy Fraction starting from the PSF worked out from the modelization in Sec. 3. For the on-axis PSF we calculate the radius enclosing 50% or 80% of the energy as a function of the energy;
- In Sec. 5 I summarize the results.

2 The data set.

The data set includes observations taken both in the commissioning phase and in calibration and performance verification phase. They concern revolutions from 27 to 57. Up to the present, I have analyzed observations of point sources whose images were completely inside the central CCD of the MOS. The offsets in respect with the on axis position vary from 0 to 2 arcmin.

Whenever it was possible, we joined different observations (just overlapping the runs) in order to enhance the statistics. We merged observations, if concerning the same point source, with the same observation position, the same operative mode, the same filter etc.

The sources used for the calibrations are: Capella, HR1099, EXO0748-67, GX13+1, LMC X-3, PKS0312, PKS0558-504 and PSR0540.

A large fraction of the observed sources have a count rate high enough to induce pile-up effects. In these cases, we don't have any information about the core of the PSF, but the wings can be studied. If a corresponding observation (same source and pointing position but different filter and/or operative mode, i.e. different pile-up) exists, we can study simultaneously the core and the wings. Often only piled-up data are available.

As a result, we will have a very precise estimate of the slope of the PSF, but a poorer evaluation of the core radius.

As PSF depends on energy, we divided the whole spectral range [0-10 keV] in different intervals: $[200, 400], [400-800], [800-1200], [1200-2400], [2400-5000], [5000-8000], [8000-12000]$ eV, corresponding to mean energies $0.3, 0.6, 1, 1.8, 3.7, 6.5, 10$ keV.

3 Modeling the PSF

According to the ground calibration, the PSF could be fitted with a $King + Gauss$ function:

$$PSF = A\left\{\frac{1}{\left[1+\left(\frac{r}{r_c}\right)^2\right]^{\alpha}} + \frac{R}{\sqrt{(2\pi\sigma^2)}}\exp\left[-\left(\frac{r}{\sigma}\right)^2\right]\right\} \tag{1}$$

with 4 free parameters to be determined fitting the data:

- r_c: the core radius of the (main) King component;
- α: the King slope;
- σ: the Gaussian amplitude;
- R : the relative normalization of the two components.

The parameters depend on energy and off axis angle. The total normalization A depends on the total flux of the observation.

From ground calibration (on data concerning FM1) the values of the parameters where at 1.5 keV

$$r_c = 6.062 \pm 0.582$$

$$\alpha = 1.748 \pm 0.021$$

$$\sigma = 126.74 \pm 3.09$$

$$R = 2.69 \cdot 10^{-2} \pm 8.25 \cdot 10^{-3}$$

(see S.G. EPIC-MCT-TN-001, http://www.ifctr.mi.cnr.it/~simona/pub for details) Ground calibrations concerned the FM1 which is a spare camera. The parameters reported herebelow can not be compared with the present analysis because they refer to a different CCD.

For in orbit data actually the presence of the X background hides the gaussian component and the fitting becomes insensitive to the gaussian parameters. For this reason, we are obliged to neglect the presence of the gaussian component and the fitting curve is reduced to the King profile:

$$PSF = A \left\{ \frac{1}{\left[1 + \left(\frac{r}{r_c}\right)^2\right]^{\alpha}} + BKG \right\} \tag{2}$$

A constant modeling the background has been added.

3.1 Grouping similar observations

We joined together observations having the following requirements:

1. same source target;
2. same pointing direction;
3. same operation mode (FF, DN, LW, SW);
4. same filter position.

Obviously we merged together observations separately for the two MOS cameras.

After this merging operation, we divided the data into groups. Merged data sets concerning the same target and with the same pointing position but with different operation mode and/or filter position, i.e. with different pile-up levels, are included in the same group. We identified 47 (24 concerning the MOS 1 and 23 the MOS 2) groups each having the same source target and the same pointing position (i.e. the offset).

We applied to each group, for each energy band a fitting procedure able to fit simultaneously different curves having different pile-up levels, constraining the fit parameters r_c and α to be the same for all the profiles of the group. Of course, the total normalization and the background constant are different for the different curves. Hence, we worked out a number of best fit parameters as functions of the offset angle and of the energy.

In figure 1 we report as an example the simultaneous fit of a PSF image on the MOS 2, for three curves having three different pile-up levels. The source target is LMC X-3. The energy range selected corresponds to a mean energy value of 1.8 keV. The centroid of the image is (358, 219) in CCD pixel coordinates corresponding to an offset angle of 1.78 arcmin. The three curves refers to

- Double Node with filter Thin: this corresponds to the black curve in figure with no pile-up effects;
- Large Window with filter Medium: this corresponds to the blue curve in the figure with some pile-up;
- Full Frame with filter Medium: this correspond to the yellow curve in the figure with the higher level of pile-up.

The best fit parameters derived using the simultaneous fitting procedure are:

$$r_c = 5.591 \pm 0.079$$

$$\alpha = 1.449 \pm 0.006$$

In figure 2 we report the fit for an observation of the same source and the same energy range but with an on-axis pointing: the centroid coordinates are (308, 299) - CCD pixels units - corresponding to an offset angle of 0.08 arcmin. The three curves correspond to

- Small Window with filter Medium: the curve is the merging of two different observations: pile-up is substantially absent (black curve);
- Large Window with filter Medium: the curve is the merging of two different observations: some pile-up is present (blue curve);
- Full Frame with filter Medium with the higher level of pile-up (yellow curve).

The corresponding best fit parameters are:

$$r_c = 4.111 \pm 0.034$$

$$\alpha = 1.415 \pm 0.005$$

The same procedure has been applied to each group for each energy band. A set of best fit parameters (depending on energy and on offset angle) for each MOS has been worked out.

3.2 The core radius and the slope as functions of the energy

For each group (and correspondingly for each offset angle) we can derive the core radius and the slope as a function of the energy. In the figures 3 and 4 we reported the case of an observation of LMC X-3 on MOS 1, for an offset angle of 1.65 arcmin. The energy is

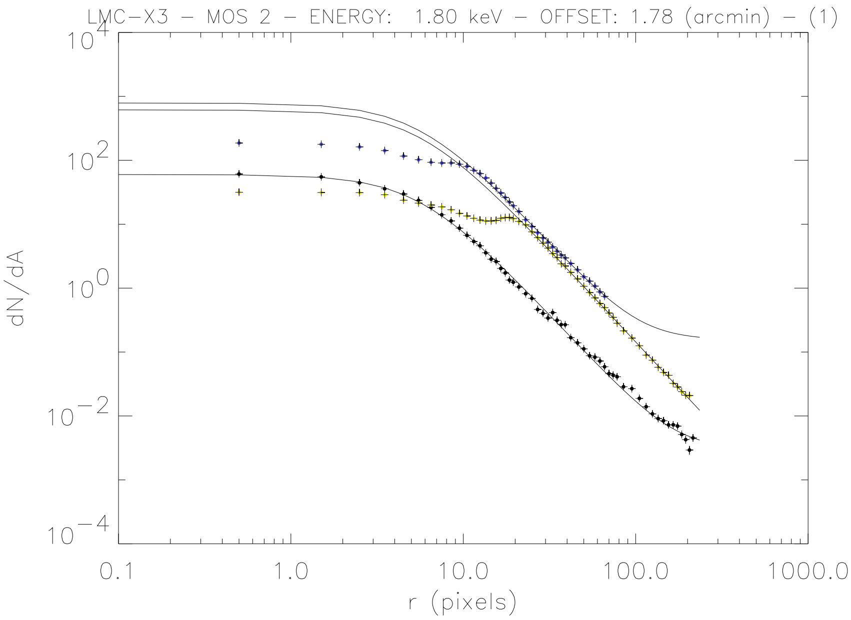

Figure 1: Simultaneous fit of three radial profiles having three different pile-up levels. The observations refer to LMC X-3 with an offset angle of 1.78 arcmin.The selected energy range corresponds to a mean energy of 1.8 keV.

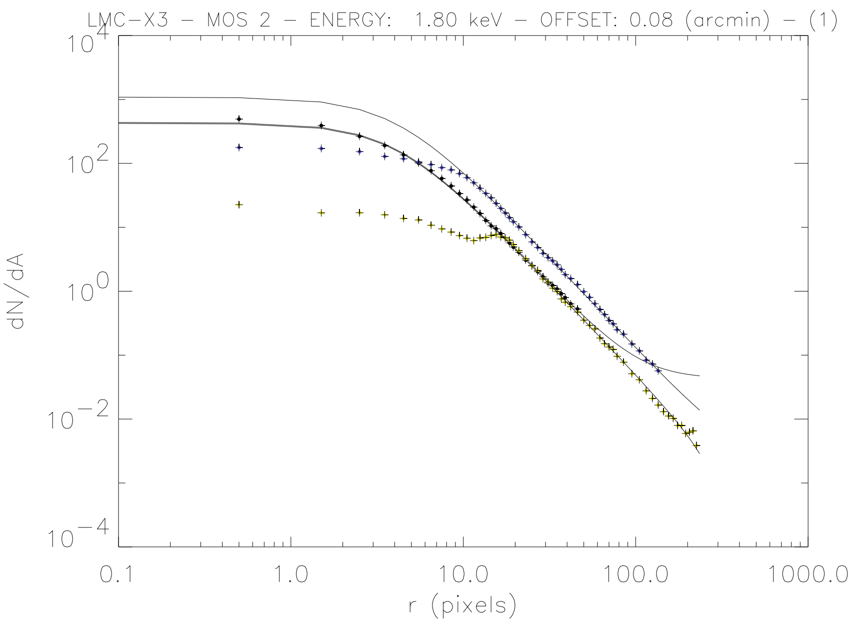

Figure 2: Simultaneous fit of three radial profiles having three different pile-up levels. The observations refer to LMC X-3 with an offset angle of 0.08 arcmin.The selected energy range corresponds to a mean energy of 1.8 keV.

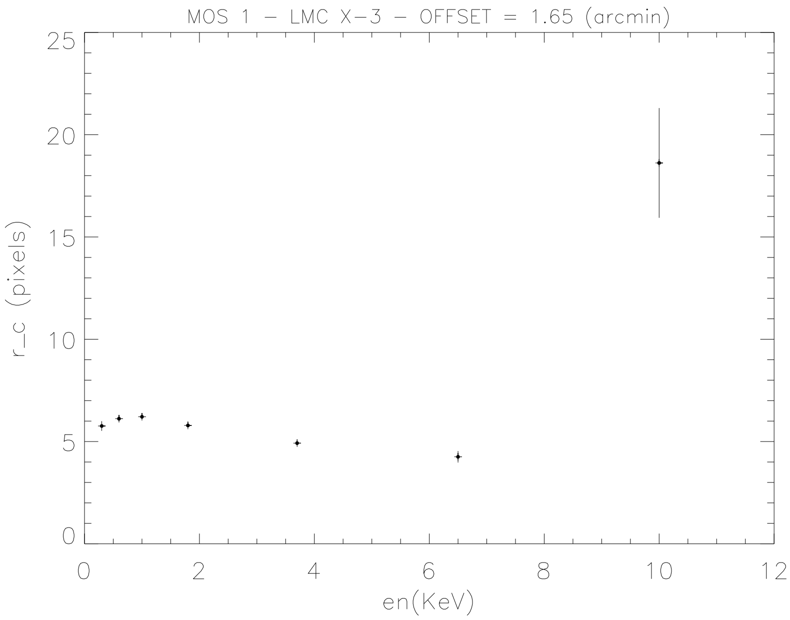

Figure 3: King core radius as a function of the energy. The values have been obtained fitting the radial profile at different energies of observations of LMC X-3 with the MOS 1 at an offset angle of 1.65 arcmin.

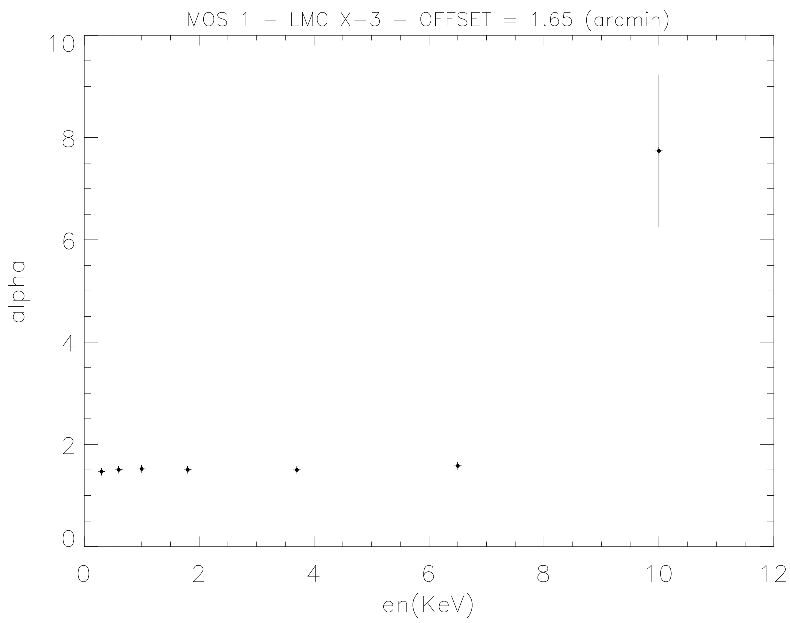

Figure 4: King slope as a function of the energy. The values have been obtained fitting the radial profile at different energies of observations of LMC X-3 with the MOS 1 at an offset angle of 1.65 arcmin.

given in keV and the core radius is in pixels unit (1 pixel= $1.1''$). From fig. 3 it can be seen that the core radius tends to decrease when energy increases. The general decreasing trend of the core radius is expected as the photons with higher energy will be reflected and focused only by the inner shells of the X–ray telescope. The reduced number of involved shells diminishes the source of "dispersion"; furthermore, the inner shells are probably less irregular. Both these effects improve the ability of focusing by the telescope with increasing energy. So the core radius is expected to be slightly smaller for higher energy photons. In fig. 4 the slope versus energy is represented. The slope seems to be constant, with a slightly tendency to decrease. This is also expected as high energy photons have a wavelength nearer to the roughness size of the telescope shells than low energy photons, with an enhanced probability of scattering processes. This effect gives prominence to the wings of the PSF, which become, for higher energies, more important.

Nevertheless, both in fig. 3 and in fig. 4, it can be seen that the last point, at 10 keV is very high. Furthermore, in fig. 3, the two first points at energies $\lesssim 1$ keV show a displacement from linear trend and slightly increase with energy. Note that the first feature is not so evident in 4 as the slope does not vary so significantly with the energy. It is worth to discuss in detail these two different features.

The point at 10 keV corresponds to the best fit in fig. 5, where statistics is not enough to make the fitting reliable. Such a point must be rejected.

The displacement observed for the first two points can be explained by looking at the spectrum of this source, shown in fig. 6. For energies $\lesssim 1$ keV, the spectrum is absorbed. Photons in the lower part of the spectrum are actually photons of higher energies; their contribution in the spectrum at low energies is due to the limited energy resolution. For those observations having an absorbed spectrum, data at low energies must not be considered.

3.3 The core radius and the slope as functions of the offset angles.

For each energy we can consider all the different observations having different pointings (i.e. offset angles) and we can plot the core radius and the slope as functions of the offset angles (see figs. 7 and 8).

The variation of the two parameters with the energy is quite small. Some points are displaced from the general trend. Such points have been investigated and in fig. 9 we show the radial profile and the best fit for the point having offset 0.12 and $r_c = 64.501 \pm 9.975$ and $\alpha = 3.081 \pm 0.469$ at 1.8 keV. From the figure it can be seen that the radial profile is strongly affected from pile-up. No data are recorded at radii lower than 20 pixels and the radial profile never reaches the unity. The procedure of fitting fails to converge after

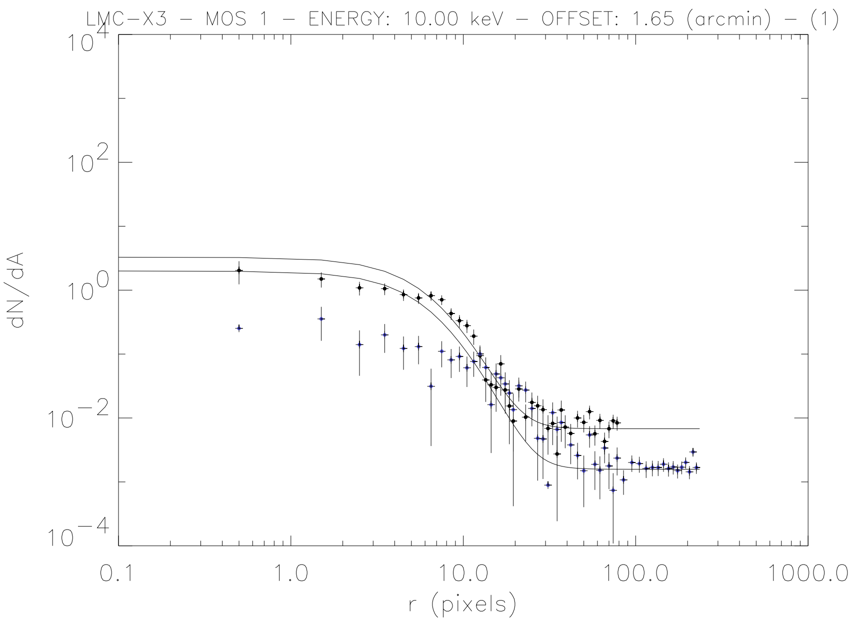

Figure 5: Radial profiles and best fits for observations of LMC X-3 on MOS 1 at 10 keV at an offset angle of 1.65 arcmin. Different curves refer to different pile-up levels. The statistics is not enough to make the fit reliable.

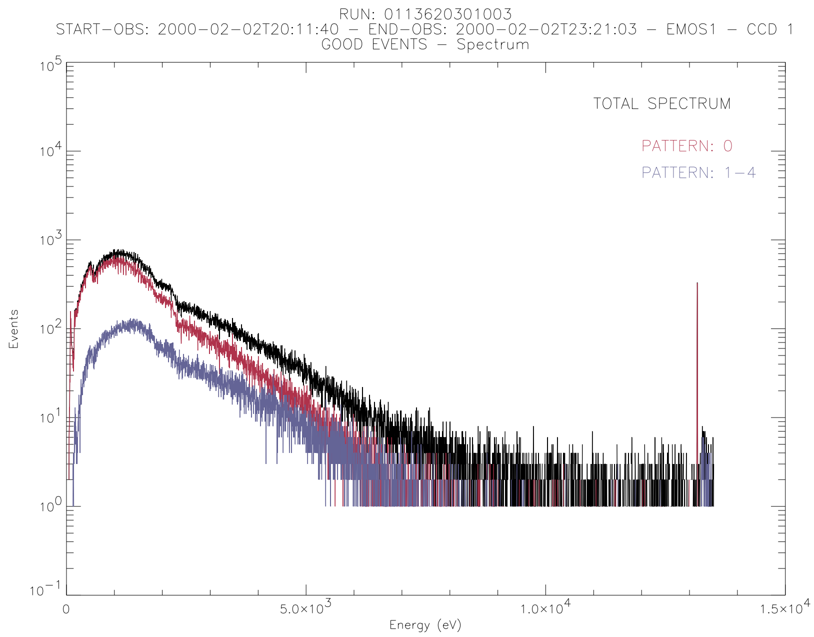

Figure 6: Spectrum of an observation of LMC X-3. For energies $\lesssim 1$ keV the spectrum is absorbed.

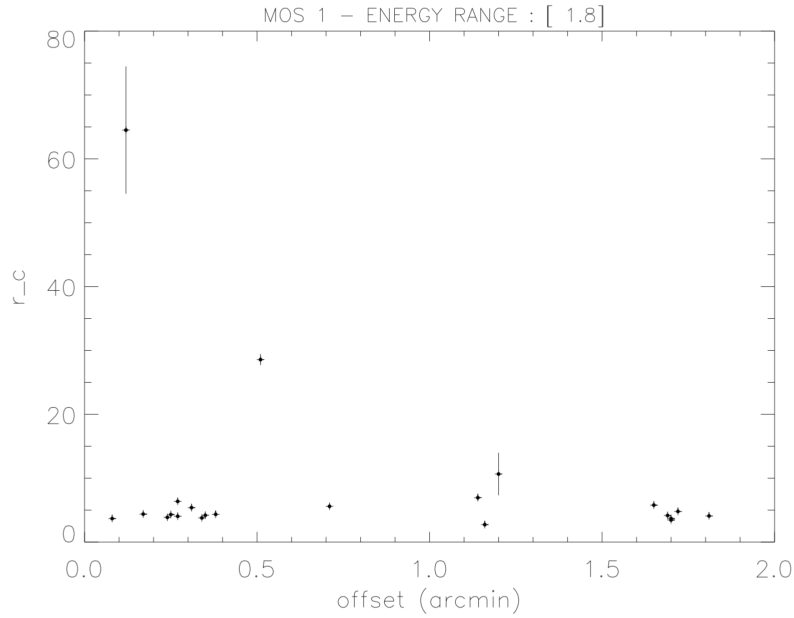

Figure 7: King core radius as a function of the offset angles. The values have been obtained fitting the radial profiles of all the observations at the energy of 1.8 keV. Data refers to MOS 1.

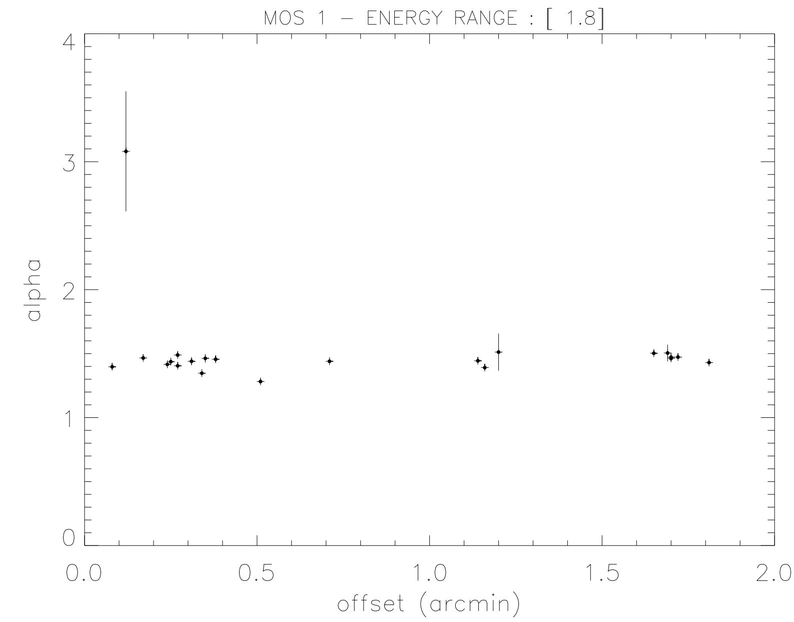

Figure 8: King slope as a function of the offset angles. The values have been obtained fitting the radial profiles of all the observations at the energy of 1.8 keV. Data refers to MOS 1.

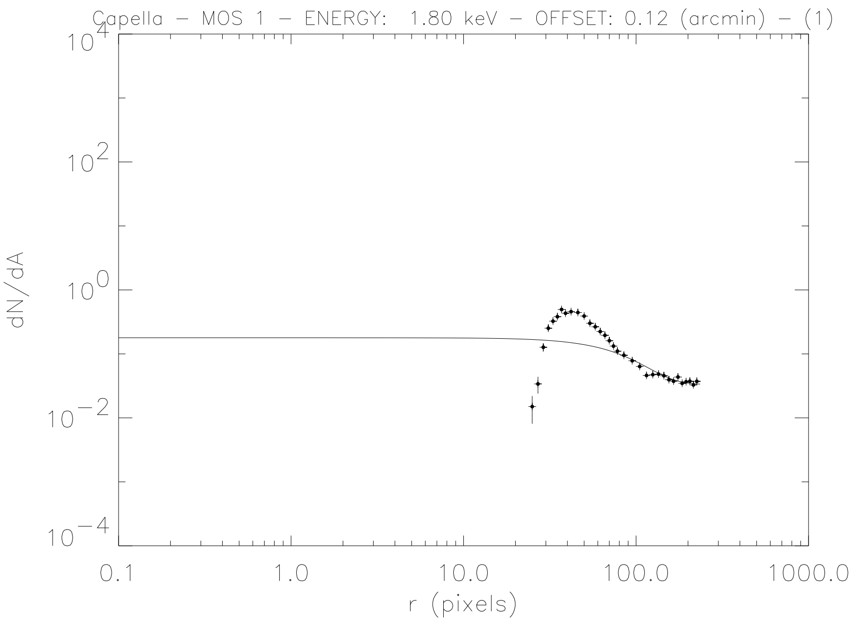

Figure 9: Radial profile and "fit" curve for an observation of Capella on MOS 1 with an offset angle of 0.12 arcmin. The selected energy is 1.8 keV. Data suffer of a strong pile-up level and the statistics is very low. Fitting procedure does not converge and the returned values do not match the data.

a large number of iterations and the values returned do not match the data. Such point is to be rejected.

The same check is made on all the fitting curves and "non-fitting" parameters are excluded. Sometimes this problem concerns only the core radius. If only a piled-up profile is available and the statistic is reasonably high, the wings can be modeled even if the core radius is not. In this case we reject only the r_c value and keep the corresponding α.

3.4 King core radius and slope as functions of energy and offset angle, after rejecting "bad" data.

After rejecting all the data affected by one of the previously described problems, the general trend of the King core radius and the slope are represented in figs 10 – 13. In figs. 10 and 11, we report the case of PKS0558-504 on MOS 1 as it is the case where the greatest quantity of points are kept after the rejections. The offset angle is 0.24 arcmin. Either the core and the slope decrease when energy increases as expected. When the energy is fixed (as an example we choose again 1.8 keV) the behavior of the parameters is shown in figs. 12 and 13. The core radius tends to increase when we move at larger

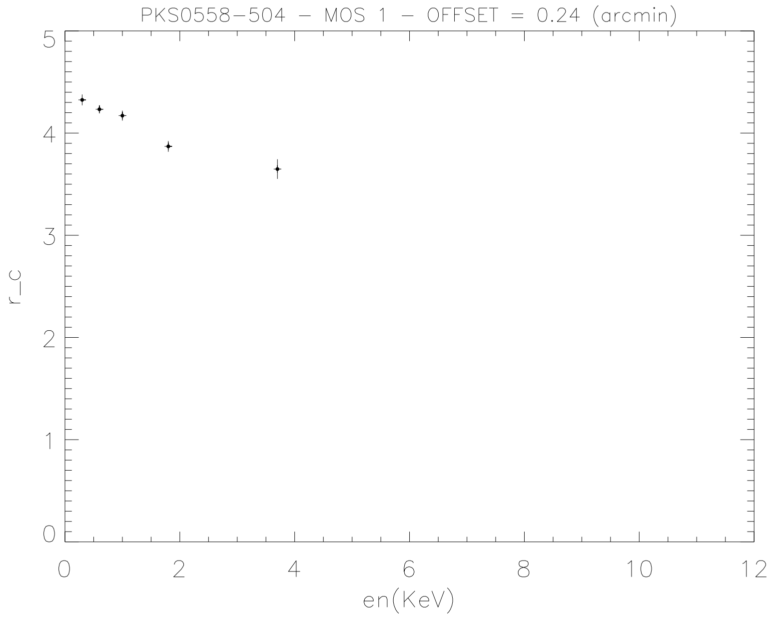

Figure 10: King core radius as a function of the energy. The values have been obtained fitting the radial profile at different energies of observations of PKS0558-504 with the MOS 1 at an offset angle of 0.24 arcmin.

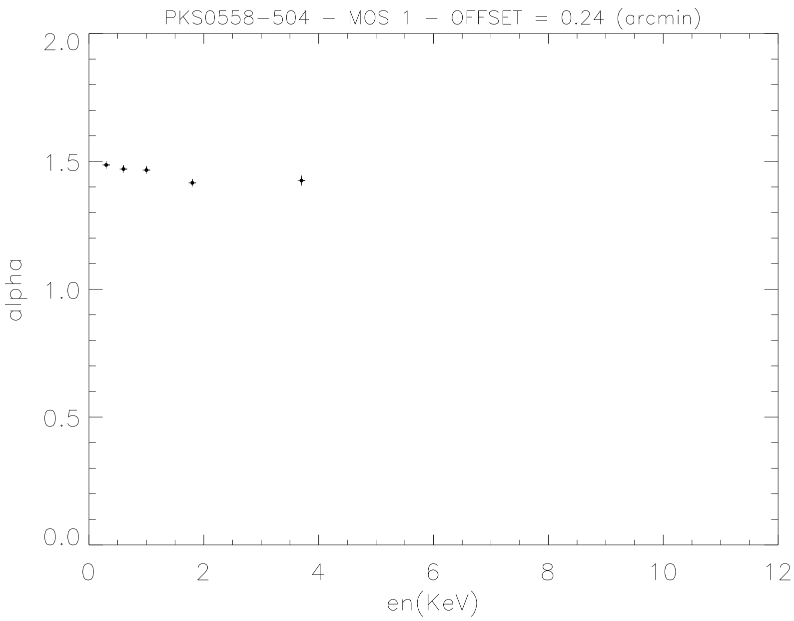

Figure 11: King slope as a function of the energy. The values have been obtained fitting the radial profile at different energies of observations of PKS0558-504 with the MOS 1 at an offset angle of 0.24 arcmin.

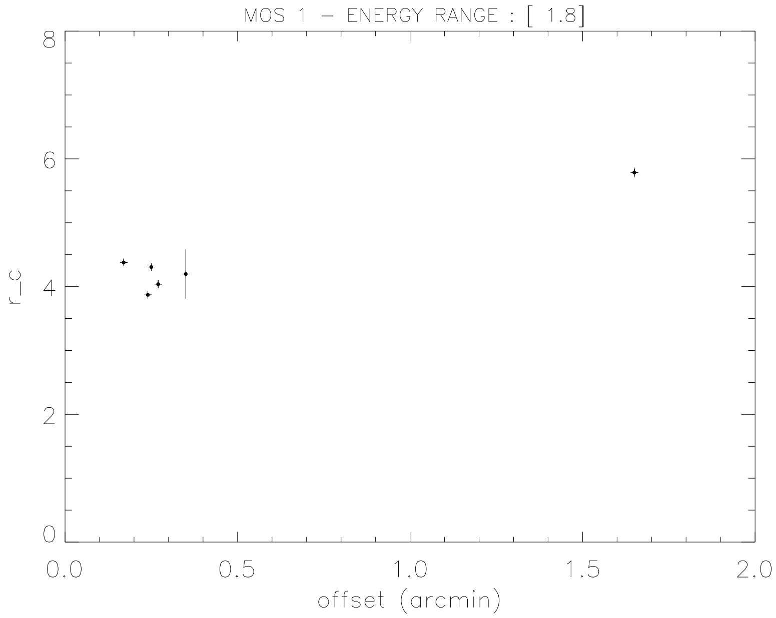

Figure 12: King core radius as a function of the offset angles. The values have been obtained fitting the radial profiles of all the observations at the energy of 1.8 keV. Data refers to MOS 1.

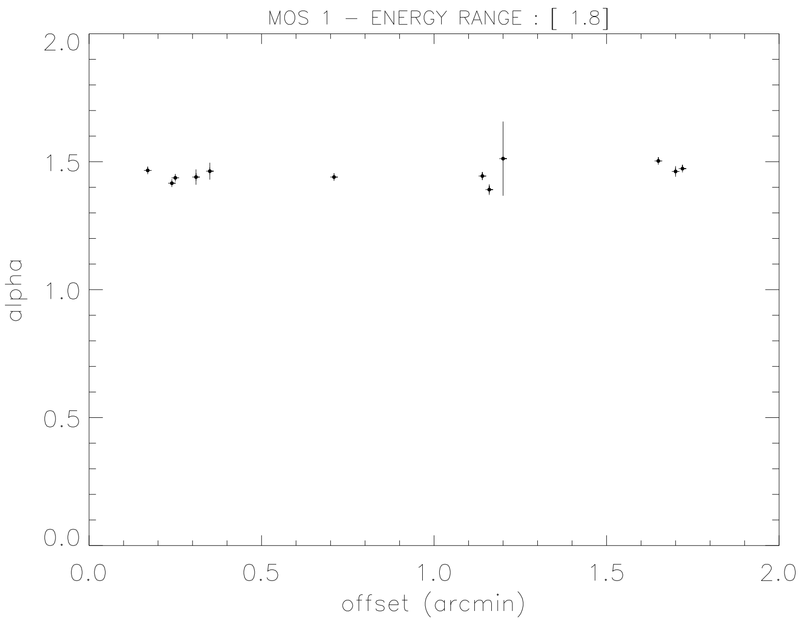

Figure 13: King slope as a function of the offset angles. The values have been obtained fitting the radial profiles of all the observations at the energy of 1.8 keV. Data refers to MOS 1.

off-axis angles, while the slope seems to remain almost constant.

Of course, the reported figures are just some examples, but the general trend of the two parameters as functions of the energy and of the offset angle is valid in all the cases. We can conclude that, whenever one of the two independent variables (energy or offset angle) is fixed, r_c and α vary linearly with the other variable. More precisely:

$$\left.\frac{\partial r_c}{\partial En}\right|_{offset} = A = constant$$
$$\left.\frac{\partial r_c}{\partial Offset}\right|_{En} = B = constant$$

Similar equations are valid for α. By means of simple integrations, it can be seen that

$$\mathrm{r_c(En, Offset) = a + b * En + c * Offset + d * En * Offset} \tag{3}$$

and analogously

$$\mathrm{\alpha(En, Offset) = x + y * En + z * Offset + w * En * Offset} \tag{4}$$

Fitting the available set of r_c and α with such relations we obtained the following values:

Table 1: r_c and α best fit according to eqns. (3) and (4)

	MOS 1			
r_c	a = 4.476 ± 0.029	b = -0.234 ± 0.015	c = 1.091 ± 0.075	d = -0.063 ± 0.030
α	x = 1.463 ± 0.004	y = -0.012 ± 0.002	z = 0.010 ± 0.004	w = 0.006 ± 0.002
	MOS 2			
r_c	a = 3.945 ± 0.003	b = -0.086 ± 0.008	c = 1.006 ± 0.053	d = -0.142 ± 0.025
α	x = 1.415 ± 4.e-4	y = 2.614e-4 ± 0.001	z = 0.013 ± 0.003	w = -0.008 ± 0.002

The fitting is performed considering the energy in keV units and the offset angles in arcmin units. The coefficients a and x gives the order of magnitude of r_c and α respectively. The other coefficients give the variations with energy and off-axis positions.

In figs. 14–17 we draw the parameters r_c and α either in a 3d plot and in a contour plot. It can be seen that the variations of α is quite small. It has a tendency to increase

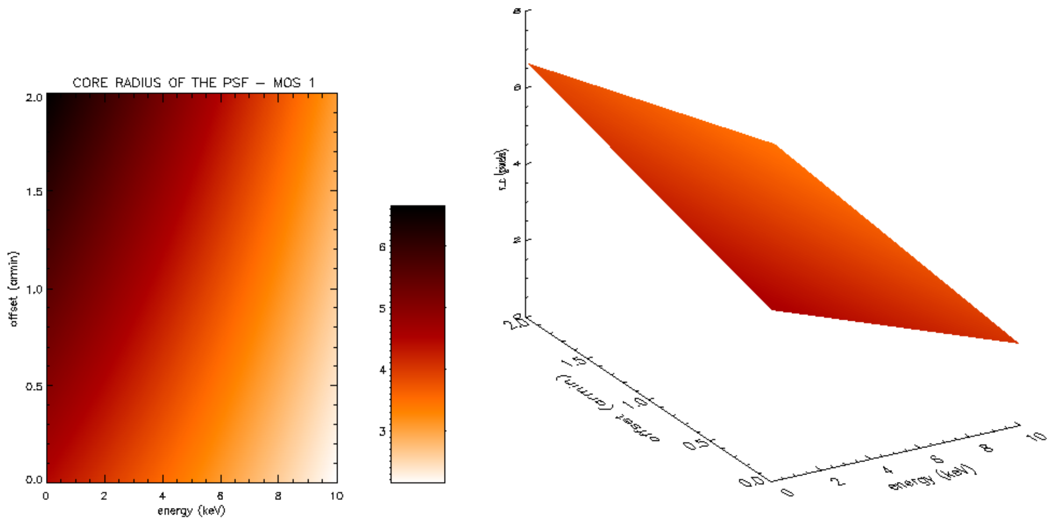

Figure 14: King core radius as a function of the offset angles and energies for MOS 1.

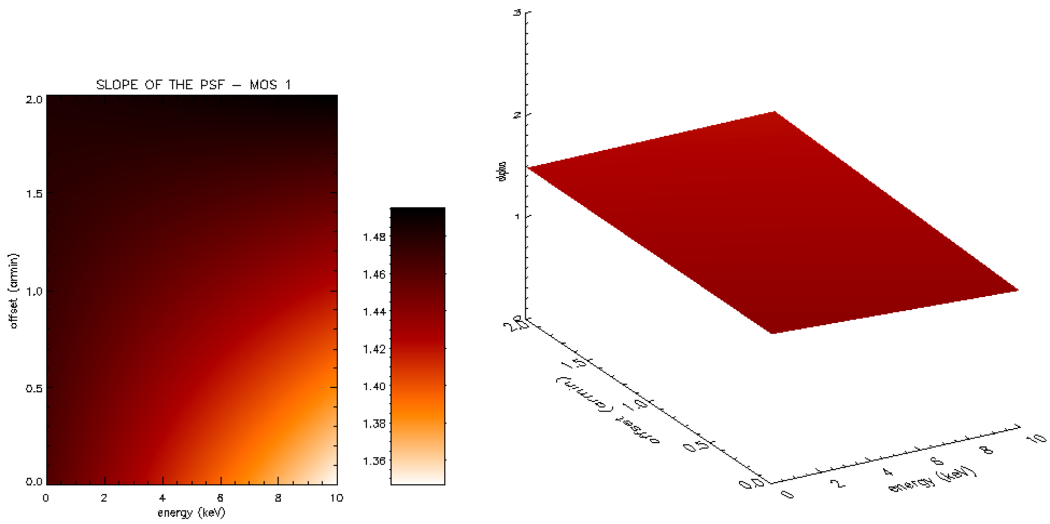

Figure 15: King slope as a function of the offset angles and energies for MOS 2.

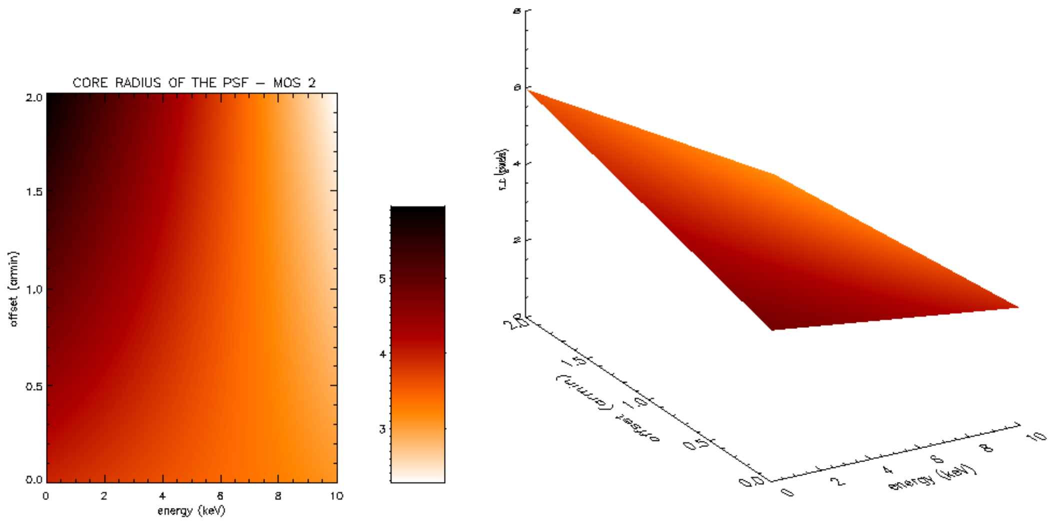

Figure 16: King core radius as a function of the offset angles and energies for MOS 2.

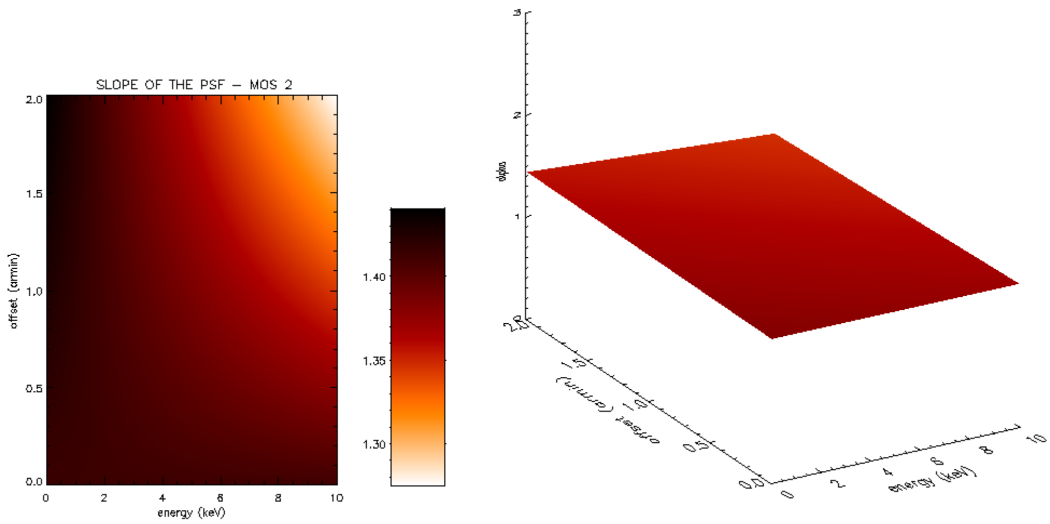

Figure 17: King slope as a function of the offset angles and energies for MOS 2.

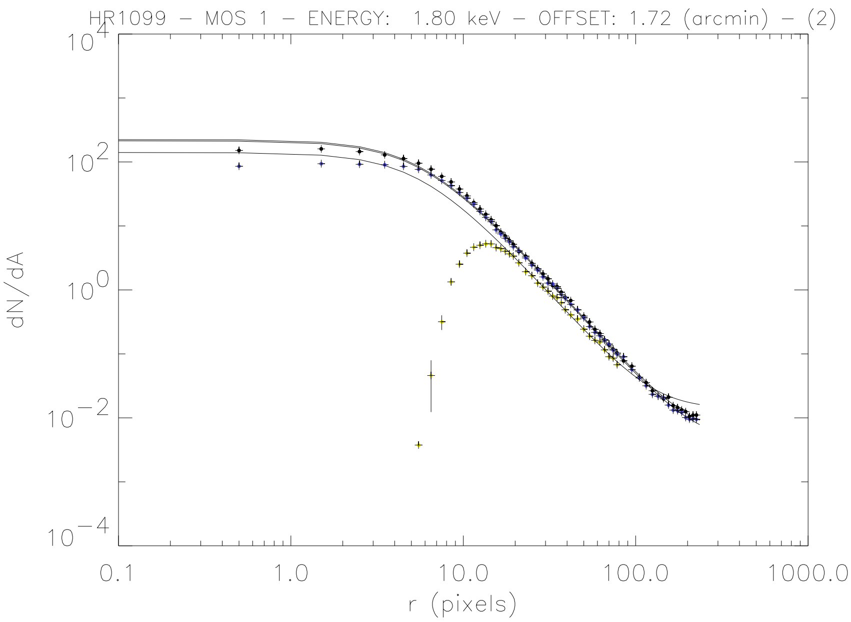

Figure 18: Data referring to observations of HR1099 at 1.72 arcmin off-axis position. Solid lines are the fit with r_c and α are fixed according to the Table 1.

at higher energies and low (high) offsets for MOS 1 (MOS 2). It is worth to notice nevertheless that the variations are modest.

In figs. 18 and 19 we report as an example the curves of some observations (with, as usual different pile-up levels) with the final King profiles. The superimposed curves ARE NOT the best fit of the data points. They are the final King profile with the parameters determined above. Only the total normalization and the background which vary curve by curve, are free parameters. The core and the slope are fixed according to the selected energy and the offset angle of the observation (see table hereabove).

It can be seen that the accordance for the slope is really very good. The core is less precise but we can see that also when only pile-up measurements are available (see fig. 19) the profile seems to be reliable.

4 Encircled Energy Fraction

An important quantity characterizing the PSF is the Encircled Energy Fraction, which specifies the fraction f of energy collected within a certain radius R.

This quantity is defined according to

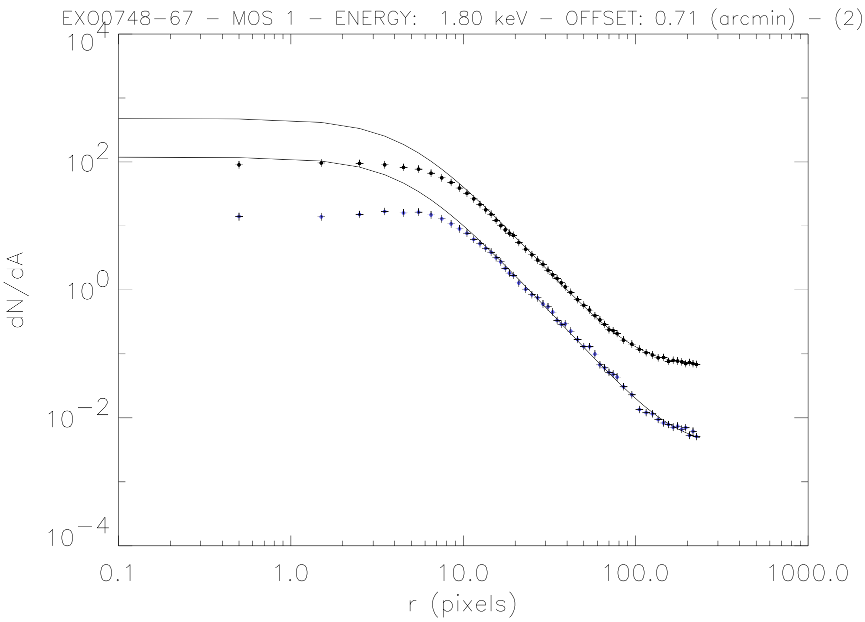

Figure 19: Data referring to observations of EXO0748-67 at 0.71 arcmin off-axis position. All the data suffer from pile-up. Solid lines are the fit with r_c and α are fixed according to the Table 1.

$$EEF(R) = \frac{\int_0^R PSF(r) r dr}{\int_0^{R_N} PSF(r) r dr}$$

R_N defines the total normalization. If we assume that the King profile holds till infinity $R_N = \infty$. Actually data profiles never go beyond 5 arcmin. For larger radii the profile is typically of the order of the background and it overcomes other components holding on the wings (e.g. the gaussian component that we saw in the ground calibration data). For this reason we decide to fix $R_N = 5$ arcmin. Using the King function (see eqn: (2))

$$EEF(R) = \frac{\int_0^R \frac{1}{\left[1+\left(\frac{r}{r_c}\right)^2\right]^\alpha} r dr}{\int_0^{5'} \frac{1}{\left[1+\left(\frac{r}{r_c}\right)^2\right]^\alpha} r dr} \tag{5}$$

This quantity can be easily be integrated and EEF can be written as follows:

$$EEF(R) = \frac{1 - \frac{1}{\left[1+\left(\frac{R}{r_c}\right)^2\right]^{\alpha-1}}}{1 - \frac{1}{\left[1+\left(\frac{5'}{r_c}\right)^2\right]^{\alpha-1}}} = f \tag{6}$$

We can compare the difference of the results on the EEF when using $R_N = 5$ arcmin or $R_N = \infty$ (which is the largest possible radius). If we measure a flux $F_{meas.}$ within a radius R the total flux F_{TOT} within R_N is, by definition:

$$F_{TOT}^{R_N} = \frac{F_{meas.}}{f(R)}$$

We can compare $F_{TOT}^{5'}$ and F_{TOT}^{∞}:

$$\frac{F_{TOT}^{5'}(R)}{F_{TOT}^{\infty}(R)} = \frac{f^{R_N=\infty}}{f^{R_N=5'}} = 1 - \frac{1}{\left[1+\left(\frac{5'}{r_c}\right)^2\right]^{\alpha-1}}$$

The two parameters r_c and α are given in eqns. (3) and (4) and in Table 1. Note that the ratio does not depend on the radius R.

For MOS 1 the ratio hereabove varies from 0.965 to 0.98 for any energy lower than 10 keV, and for MOS 2 it varies from 0.97 to 0.98. On the whole, the difference between the two estimations is of the order of 2-3%.

Starting from eqn. (6), we can easily work out the radius at which a fraction f of energy is encircled.

$$R(f; r_c, \alpha) = r_c \left\{ \left[1 - f \left(1 - \frac{1}{\left[1+\left(\frac{5'}{r_c}\right)^2\right]^{\alpha-1}} \right) \right]^{\frac{1}{1-\alpha}} - 1 \right\}^{\frac{1}{2}} \tag{7}$$

Using eqns. (3) and (4) and Table 1, for each energy and offset angle we can work out the radius including a fraction f of the energy. In figs. 20 – 23 we show the radius for EEF=0.5 and EEF=0.8 for MOS 1 and MOS 2. Considering that α is roughly constant with energy and offset, the main behavior of R is similar to r_c one.

For the on-axis position, we show in figs. 24 and 25 the radius enclosing 80% of the energy as a function of the energy, for the MOS 1 and MOS 2 respectively. The radius is plotted in pixels unit. At low energies it is roughly 23 pixels ($\sim 25''$) and it slightly decreases at larger energies ($\sim 20''$).

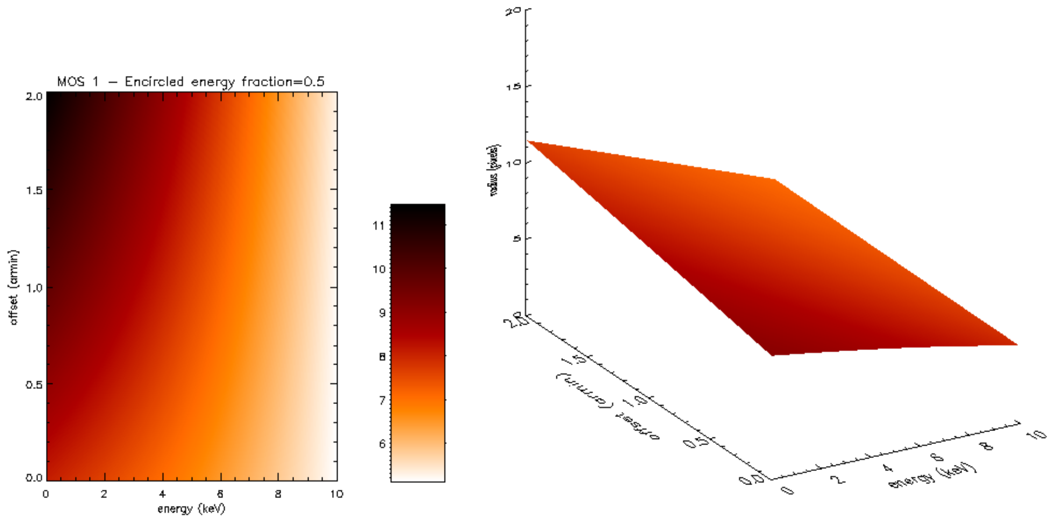

Figure 20: Radius enclosing a fraction 50% of energy (pixel units) for MOS 1.

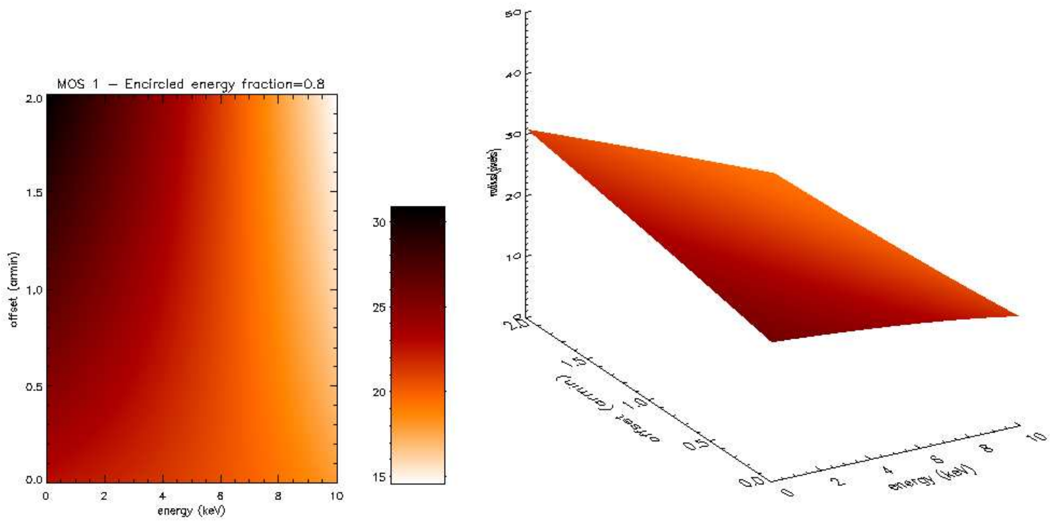

Figure 21: Radius enclosing a fraction 80% of energy (pixel units) for MOS 1.

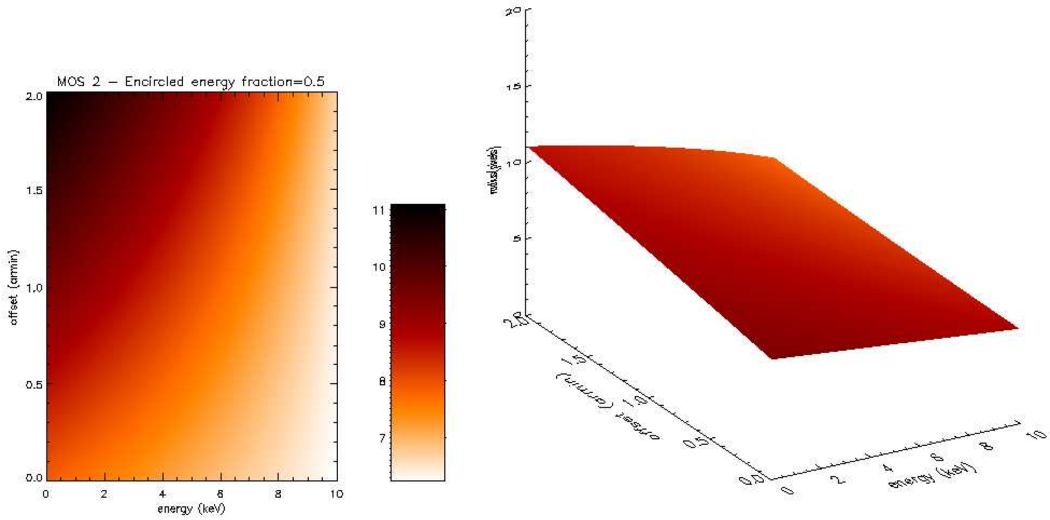

Figure 22: Radius enclosing a fraction 50% of energy (pixel units) for MOS 2.

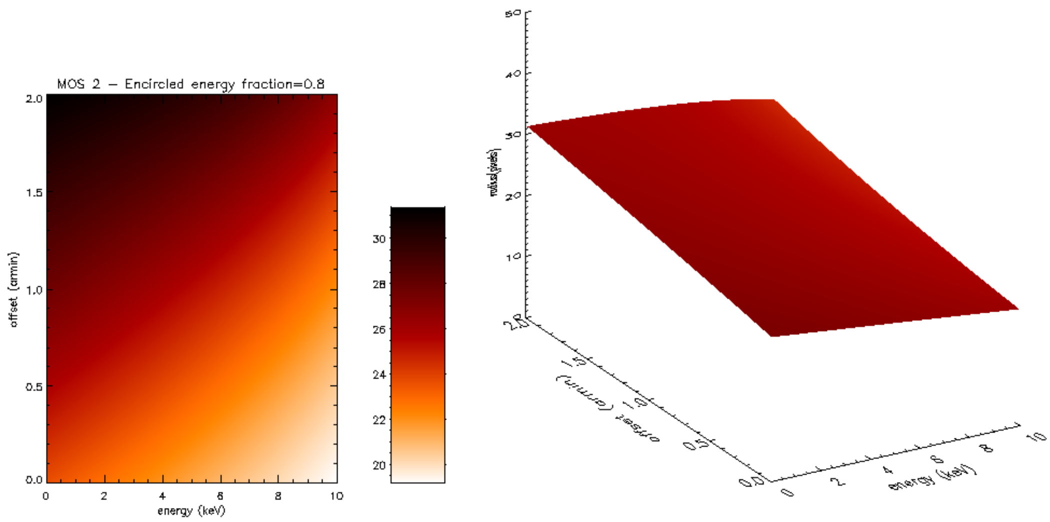

Figure 23: Radius enclosing a fraction 80% of energy (pixel units) for MOS 2.

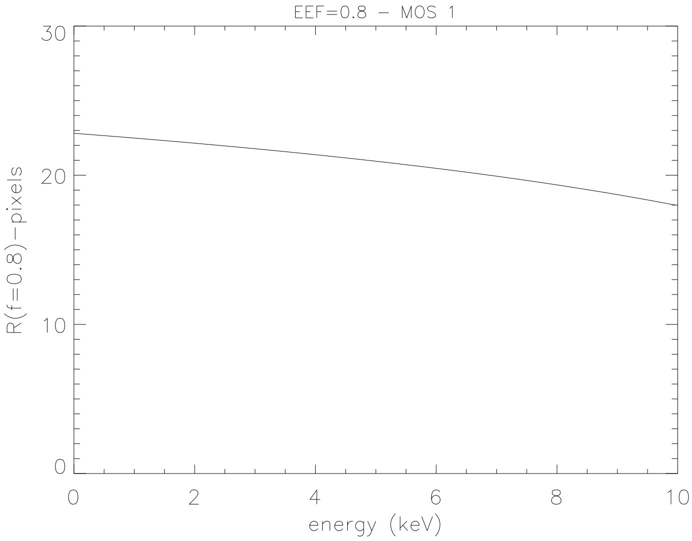

Figure 24: Radius enclosing a fraction 80% of energy (pixel units) for MOS 1.

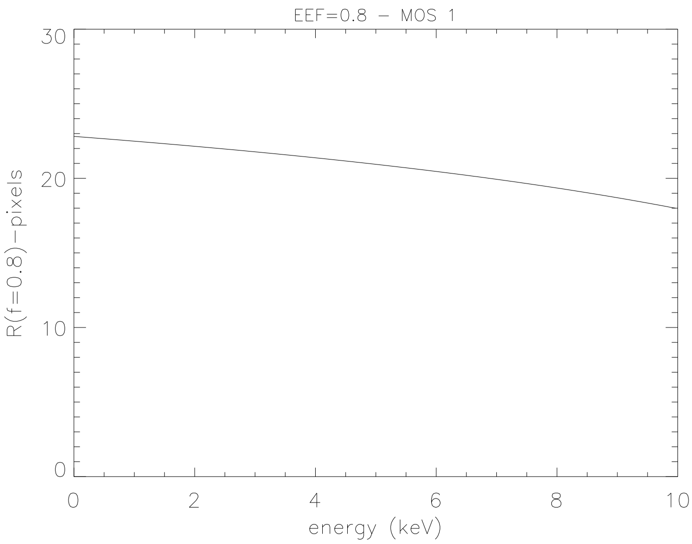

Figure 25: Radius enclosing a fraction 80% of energy (pixel units) for MOS 2.

5 Summary

In this report I present the results on the calibration of the PSF for the EPIC - MOS cameras using in-flight data. I analyzed some point sources on-axis or nearly off-axis (off-axis angles $\lesssim$ 2 arcmin), so that the source image is completely included within the central CCD.

I built the radial profiles for the observations and I built an algorithm to fit simultaneously profiles regarding the same source, the same pointing direction but different pile-up levels because of different filter position and/or operative mode.

Following the results from the ground calibration, I modeled the PSF function with a King profile, with two shape parameters (the core radius r_c and the slope of the wings α, both depending on energy and on the off-axis angle).

The core radius r_c decreases linearly when energy increases and increases with the off-axis angle. The slope parameter α is almost constant with both parameters; it slightly decreases with energy. These two parameters as functions of the energy and of the off-axis angles are reported in eqns. (3) and (4). We found the best-fit parameters for both the MOS cameras. The resulting values are provided in Table 1.

Furthermore I evaluated the Encircled Energy Fraction for both the MOS cameras, according to the definition given in eqn. (5). and I determined the radius enclosing 50% and 80% of the total light The radii enclosing 80% of the total light for the on-axis PSF as a function of the energy for the MOS 1 and MOS 2 are reported in figs. 24 and 25 respectively.